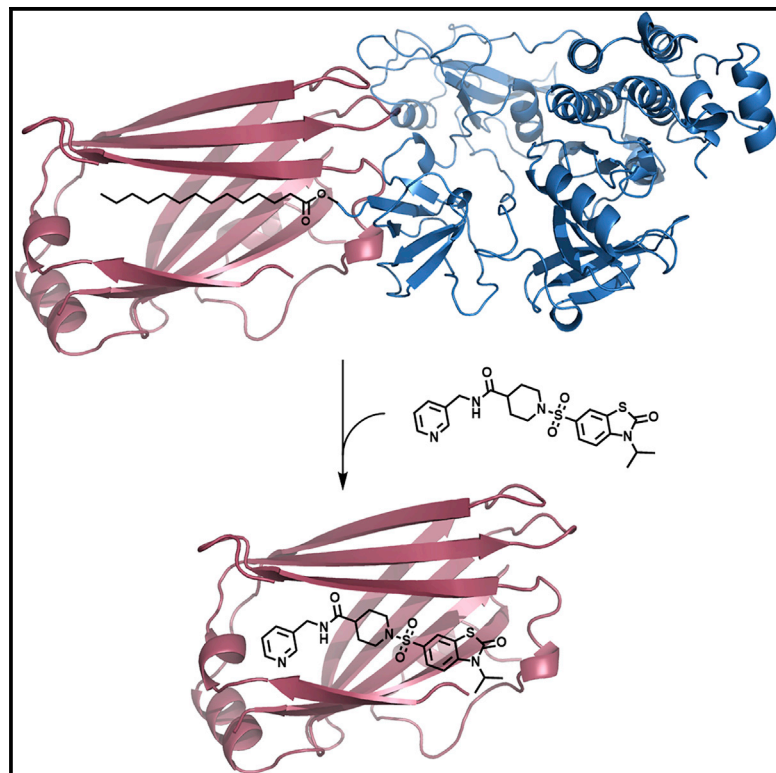


Cell Chemical Biology

Small-Molecule Inhibition of the UNC-Src Interaction Impairs Dynamic Src Localization in Cells

Graphical Abstract



Authors

Guillaume Garivet, Walter Hofer, Antonios Konitsiotis, ..., Alfred Wittinghofer, Philippe I.H. Bastiaens, Herbert Waldmann

Correspondence

philippe.bastiaens@mpi-dortmund.mpg.de (P.I.H.B.), herbert.waldmann@mpi-dortmund.mpg.de (H.W.)

In Brief

Garivet et al. discovered a small-molecule UNC119-Src interaction inhibitor, which interferes with Src enrichment at the plasma membrane and reduces clonogenic potential and growth of Src-dependent cells. Small molecule interference with the dynamics of cellular Src localization may provide an alternative approach to target oncogenic Src.

Highlights

- Identification of a structurally novel inhibitor of the UNC119-Src interaction
- Impairment of UNC119-mediated Src plasma membrane enrichment
- Reduction of activating Src Y416 autophosphorylation
- Reduction of growth and clonogenic potential of Src-dependent cells

Small-Molecule Inhibition of the UNC-Src Interaction Impairs Dynamic Src Localization in Cells

Guillaume Garivet,^{1,2,6} Walter Hofer,^{1,2,6} Antonios Konitsiotis,^{3,6} Christian Klein,^{3,6} Nadine Kaiser,^{1,2} Tom Mejuch,¹ Eyad Fansa,⁴ Rania Alsaabi,⁵ Alfred Wittinghofer,⁴ Philippe I.H. Bastiaens,^{1,3,*} and Herbert Waldmann^{1,2,7,*}

¹Department of Chemical Biology, Max-Planck-Institute of Molecular Physiology, Dortmund, North Rhine-Westphalia 44227, Germany

²Faculty of Chemistry and Chemical Biology, TU Dortmund, Dortmund, North Rhine-Westphalia 44227, Germany

³Department of Systemic Cell Biology, Max-Planck-Institute of Molecular Physiology, Dortmund, North Rhine-Westphalia 44227, Germany

⁴Structural Biology Group, Max-Planck-Institute of Molecular Physiology, Dortmund, North Rhine-Westphalia 44227, Germany

⁵Lead Discovery Center GmbH, Otto-Hahn-Straße 15, 44227 Dortmund, Germany

⁶These authors contributed equally

⁷Lead Contact

*Correspondence: philippe.bastiaens@mpi-dortmund.mpg.de (P.I.H.B.), herbert.waldmann@mpi-dortmund.mpg.de (H.W.)

<https://doi.org/10.1016/j.chembiol.2019.02.019>

SUMMARY

Interference with the signaling activity of the N-myristoylated nonreceptor protein tyrosine kinase Src is considered a viable approach in anti-cancer drug discovery. However, ATP-competitive Src inhibitors have not reached the clinic yet and alternative approaches are in high demand. The UNC119A/B proteins bind the myristoylated N terminus of Src and thereby mediate energy-driven spatial cycles that maintain Src enrichment at the plasma membrane, which is critical for Src signaling activity. We describe the discovery of a potent and specific inhibitor of the UNC119-Src interaction with unprecedented chemotype. The inhibitor binds to UNC119 in cells, and induces redistribution of Src to endomembranes and reduction of activating Src autophosphorylation on Y419. UNC119 inhibition in Src-dependent colorectal cancer cells results in the specific reduction of cell growth and clonogenic potential. Our results demonstrate that small-molecule interference with the dynamics of the Src spatial cycle may provide an opportunity to impair oncogenic Src signaling.

INTRODUCTION

The Src family kinases (SFKs) (Parsons and Parsons, 2004) are membrane-bound, signal-transducing nonreceptor protein tyrosine kinases (Parsons and Parsons, 2004). The ubiquitously expressed founding SFK member c-Src (Src) is N-terminally myristoylated and embodies two Src homology (SH) domains (SH3 and SH2), a tyrosine kinase domain, and a short C-terminal tail. A regulatory Tyr in the C terminus of Src (Y530) forms inhibitory intramolecular interactions with the SH2 domain of the protein to maintain Src in an inactive state. Dephosphorylation of Y530 by protein tyrosine phosphatases results in a conformational change and full activation of Src by means of autocatalytic

phosphorylation of Y419 in the kinase activation loop (Roskoski, 2004).

Src has been associated with multiple roles in cancer progression (Kim et al., 2009). For instance in colorectal carcinoma, Src activity increases with disease progression and is an indicator of poor clinical prognosis (Talamonti et al., 1993; Allgayer et al., 2002). Consequently, Src inhibitors targeting the kinase activity of the protein are considered potential anti-cancer therapeutics (Knight and Shokat, 2005; Breen and Soellner, 2015). However, ATP-competitive Src inhibitors may lack specificity, resulting in cytotoxicity and have not reached the clinic yet (Kim et al., 2009). Therefore, novel approaches to modulate Src activity by alternative strategies are in high demand.

The concentration of Src at the cytoplasmic face of the plasma membrane (PM) drives its self-association at the membrane and thereby the autocatalytic phosphorylation on Y419, as well as the propagation of signals by promoting the interaction with specific effectors (Bjorge et al., 2000; Barker et al., 1995). The level of Src enrichment at the PM is therefore a critical parameter for its activity, and alteration of PM-enrichment might affect oncogenic signaling by Src (Konitsiotis et al., 2017).

UNC119A and UNC119B are structurally related proteins that interact with myristoylated proteins by binding of the lipid moiety within a conserved hydrophobic pocket which also accommodates N-terminal amino acids, in particular the +2 and +3 position of cargo molecules (Wright et al., 2011; Constantine et al., 2012; Jaiswal et al., 2016). We have demonstrated that these proteins act as solubilizing factors for myristoylated SFKs, including Src, to mediate energy-driven spatial cycles that maintain SFK localization on the PM (Konitsiotis et al., 2017). These spatial cycles involve sequestration of myristoylated SFKs in the cytosol by UNC119, Arl-mediated release on perinuclear membranes and vesicular transport back to the PM. They are analogous to the spatial cycles of the farnesylated Ras proteins mediated by the GDI-like solubilizing factor, PDE6 δ (delta subunit of phosphodiesterase-6) (Chandra et al., 2011) revealing a conserved mechanism to maintain the localization of lipidated peripheral membrane molecules. Disruption of these spatial cycles in SFK-dependent colorectal cancer (CRC) cells, by knockdown of UNC119, resulted in

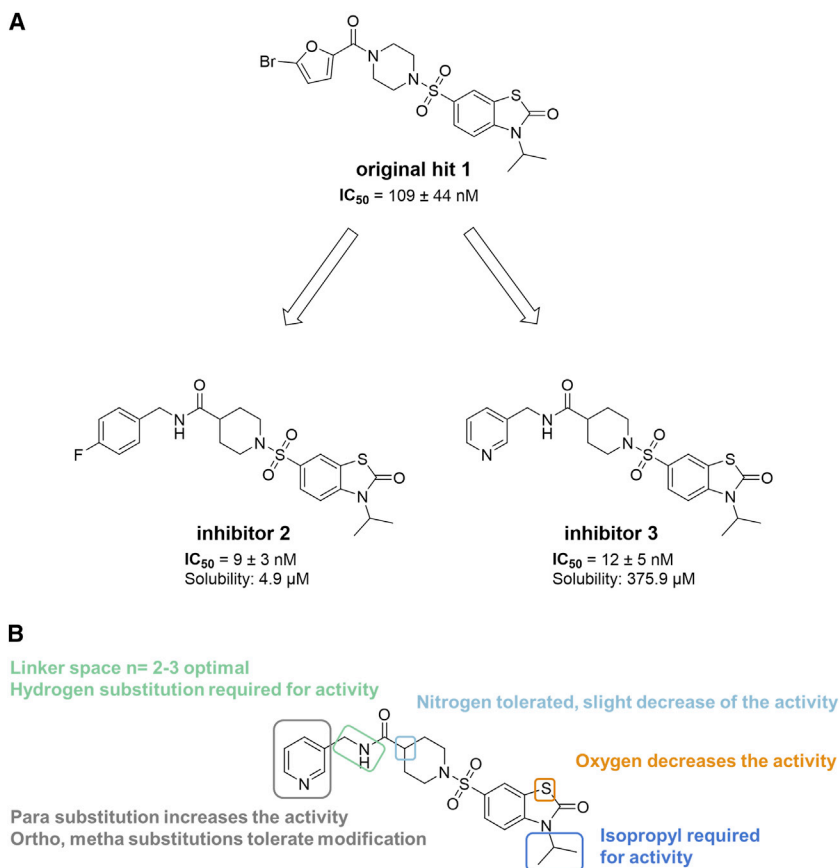


Figure 1. Benzothiazolone-Based UNC119 Inhibitors

(A) Structures of benzothiazolone inhibitors **1–3**.
(B) Structure-activity relationship leading to the development of inhibitor **3**.

tagged UNC119A protein bound to an anti-GST antibody fused to an Eu³⁺ cryptate complex is employed as a Förster resonance energy transfer (FRET) donor. A myristoylated and biotinylated N-terminal peptide, derived from the Src protein that binds to UNC119A with a K_D of 91 nM (Mejuch et al., 2015) in complex with streptavidin-d2, served as FRET acceptor (Figure S2). Inhibitors destabilize the complex, which leads to reduction of the acceptors emission. The screen revealed substituted benzothiazolones, e.g., **1** as original hit class and novel ligands for UNC119A (Figure 1A; Table S1).

While the original hit **1** was already appreciably potent, its solubility was poor, calling for improvement of compound properties through library synthesis. The synthesis of selected analogs of **1** was achieved in five to seven steps (Figure S1). Additional compounds were commercially available. In total, 40 compounds were investigated for binding to UNC119A to determine a structure-activity relationship (Figure 1B; Table S2). Representative examples are shown in Table 1. As general trends, smaller or larger N-alkyl substituents of the thiazolone or replacement of the sulfur atom by an oxygen led to less active or inactive compounds (entries **4–6**, Table 1). In addition, sulfonamides of substituted piperazines or piperidines had the most favorable properties. *para* substitution of the phenyl ring yielded the most active compounds (compare entries **8** and **9**). Increasing the distance between the phenyl ring and the piperazine moiety resulted in similar potency but did not increase the solubility of the inhibitors (entries **7**, **10**, and **11**). Introduction of N-heterocycles, in general, improved solubility (entry **3**, Table 1).

From this investigation, compound **2** emerged as a UNC ligand with low nanomolar affinity. However, compound **2** was poorly soluble (4.9 µM) and, therefore, not suitable for further biological investigation. Instead, slightly less-potent compound **3** was chosen for in-depth investigation because it combines high potency with appreciable solubility. The half maximal inhibitory concentration (IC₅₀) for displacement of the Src peptide from UNC119A (IC₅₀ = 12 nM) was ca. 10-fold improved as compared with the guiding hit. Investigation of kinetic solubility revealed that compound **3** is fairly soluble (375.9 µM). Numerous attempts to obtain a complex crystal structure were unsuccessful, and, therefore, a model for the binding mode was established by means of molecular docking (Mejuch et al., 2017).

reduction of PM localized SFKs, inhibition of SFK activity and inhibition of cell growth.

Small-molecule inhibition of the PDE6δ-KRAS interaction affects the spatial organization of KRAS and impairs oncogenic RAS signaling (Zimmermann et al., 2013; Papke et al., 2016; Martín-Gago et al., 2017a, 2017b). Following this logic, small-molecule inhibition of the UNC119-Src inhibition provides a yet-unexplored approach to interfere with the cellular localization and consequently signaling activity of Src in cells, and a first small molecule that binds to UNC119 in cell lysate and interferes with Src autophosphorylation has been reported (Mejuch et al., 2017).

Here we describe the discovery of a potent and specific UNC119 inhibitor with unprecedented chemotype. We demonstrate that the inhibitor binds to the solubilizing factor UNC119 in cells, leading to redistribution of Src to the extensive endomembrane system of the cell and resulting in reduced phosphorylation of Src. We demonstrate that UNC119 inhibition in Src-dependent CRC cells results in the specific reduction of cell growth and clonogenic potential.

RESULTS

Discovery of UNC Inhibitors

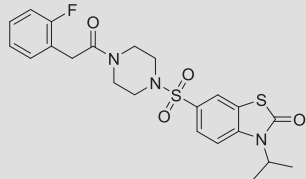
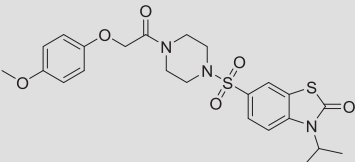
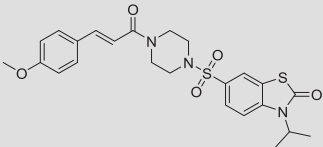
To identify UNC inhibitors, we subjected our in-house compound library (ca. 200,000 compounds) to a screening assay that monitors homogeneous time-resolved fluorescence (HTRF), as described previously (Mejuch et al., 2017). In this assay, GST-

Table 1. Evaluation of Benzothiazolone-Based Inhibitors of the Interaction between UNC119A and Myristoylated Cargo^a

Compound	Structure	IC ₅₀ (nM)	Kinetic Solubility (μM)
1		109 ± 44	ND
2		9 ± 3	4.9
3		12 ± 5	375.9
4		74 ± 9	ND
5		inactive	ND
6		129 ± 9	ND
7		18 ± 2	38.5
8		50 ± 2	ND

(Continued on next page)

Table 1. Continued

Compound	Structure	IC ₅₀ (nM)	Kinetic Solubility (μM)
9		142 ± 6	ND
10		15 ± 1	24
11		19 ± 2	10.1

^aAll data are shown as means ± SD of three independent experiments. ND, not determined. Kinetic solubility was determined as described: Inhibitors were diluted in aqueous HEPES buffer (50 mM [pH 7.4]) and incubated for 90 min while constantly stirring. Following filtration of the solution, the relative kinetic solubility of test compounds in aqueous buffer was calculated by measuring the spectrophotometric absorbance between 250 and 500 nm and comparing the recorded absorbance value with the absorbance of the compound in the 50% acetonitrile solution.

Binding Selectivity

To determine whether ligand **3** selectively targets UNC119A, its possible binding to the farnesyl-protein binding proteins PDE6δ (Zhang et al., 2004), AIPL1 (Majumder et al., 2013), and calmodulin (Sperlich et al., 2016), as well as the geranylgeranyl-protein binding protein RhoGDI (Keep et al., 1997) was investigated (Figure 2) by means of a fluorescence polarization assay. In this assay, fluorescent-labeled peptides representative for the respective cargo were chosen. These are the three myristoylated peptides characteristic for Src, Lyn, and RP2, for UNC119A and the S-farnesylated Rheb-peptide for PDE6δ, AIPL1, and calmodulin or a geranylgeranyl Rab peptide (Chen et al., 2010) for RhoGDI. Binding of the myristoylated peptides to the specific binding partner led to an increase of the fluorescence polarization signal. In contrast, competitive binding of the small-molecule ligand induced release of bound peptide and thereby reduction of the polarization signal. Figure 2A shows that an excess of compound **3** selectively released all N-myristoylated peptides from UNC119. The inhibitor displaced both the peptide characteristic for the high-affinity binding partner RP2 as well as the peptides characteristic for the lower-affinity binding partners Src and Lyn with comparable efficiency. No displacement of the lipidated cargo from the farnesyl binding proteins PDE6δ, calmodulin, and AIPL1 was detected. In addition, no displacement of a geranylgeranylated peptide from the geranylgeranyl binding protein RhoGDI was observed (Figure 2A). Thus compound **3** selectively targets the interaction between UNC119A and its myristoylated cargo proteins.

Target Engagement

The homologous proteins UNC119A and B have very similar affinity to Src peptides (Jaiswal et al., 2016). The interaction of

compound **3** with both UNC119A and B was further characterized in a complex cytoplasmic lysate environment by means of a cellular thermal shift assay (CETSA) (Franken et al., 2015; Reinhard et al., 2015). This assay monitors the thermal stabilization of the UNC119 proteins on binding to the ligand. Tandem mass spectrometry analysis revealed stabilization of UNC119A and UNC119B in Jurkat cell lysate on being treated with compound **3** (Figure 2B), with a significant thermal shift of $\Delta T = 2.4^\circ\text{C} \pm 0.8^\circ\text{C}$ for UNC119A and $\Delta T = 6.2^\circ\text{C} \pm 0.7^\circ\text{C}$ for UNC119B. We could not observe any stabilization or destabilization of PDE6δ under these conditions, which confirms again selectivity of **3** for both UNC119 isoforms.

The interaction between myristoylated Src protein and UNC119 in live cells was measured by means of fluorescence lifetime imaging microscopy of FRET (FLIM-FRET) (Konitsiotis et al., 2017). HeLa cells were transiently transfected with a mutant Src protein in which the positively charged amino acids of Src's polybasic C-terminal stretch are mutated to polar, uncharged Gln, C-terminally fused to mCitrine (Src^{6Q}-mCit) (Konitsiotis et al., 2017), and with UNC119A or UNC119B C-terminally fused to mCherry (UNC119A-mCh and UNC119B-mCh, respectively). The Src^{6Q}-mCit mutant distributes to all membranes in the cell because of its rapid exchange between membrane surfaces and the cytosol. Indeed, upon co-expression of both UNC119-mCh variants it exhibited a homogeneous interacting fraction and solubilization in the cytoplasm (Figure 3A), and is therefore well suited to measure small-molecule displacement of myristoylated Src proteins from UNC119 by FLIM-FRET (Konitsiotis et al., 2017).

Increasing concentrations of **3** resulted in a reduced interaction of Src^{6Q}-mCit with UNC119-mCh that was paralleled by a redistribution of Src^{6Q}-mCit from the cytosol to

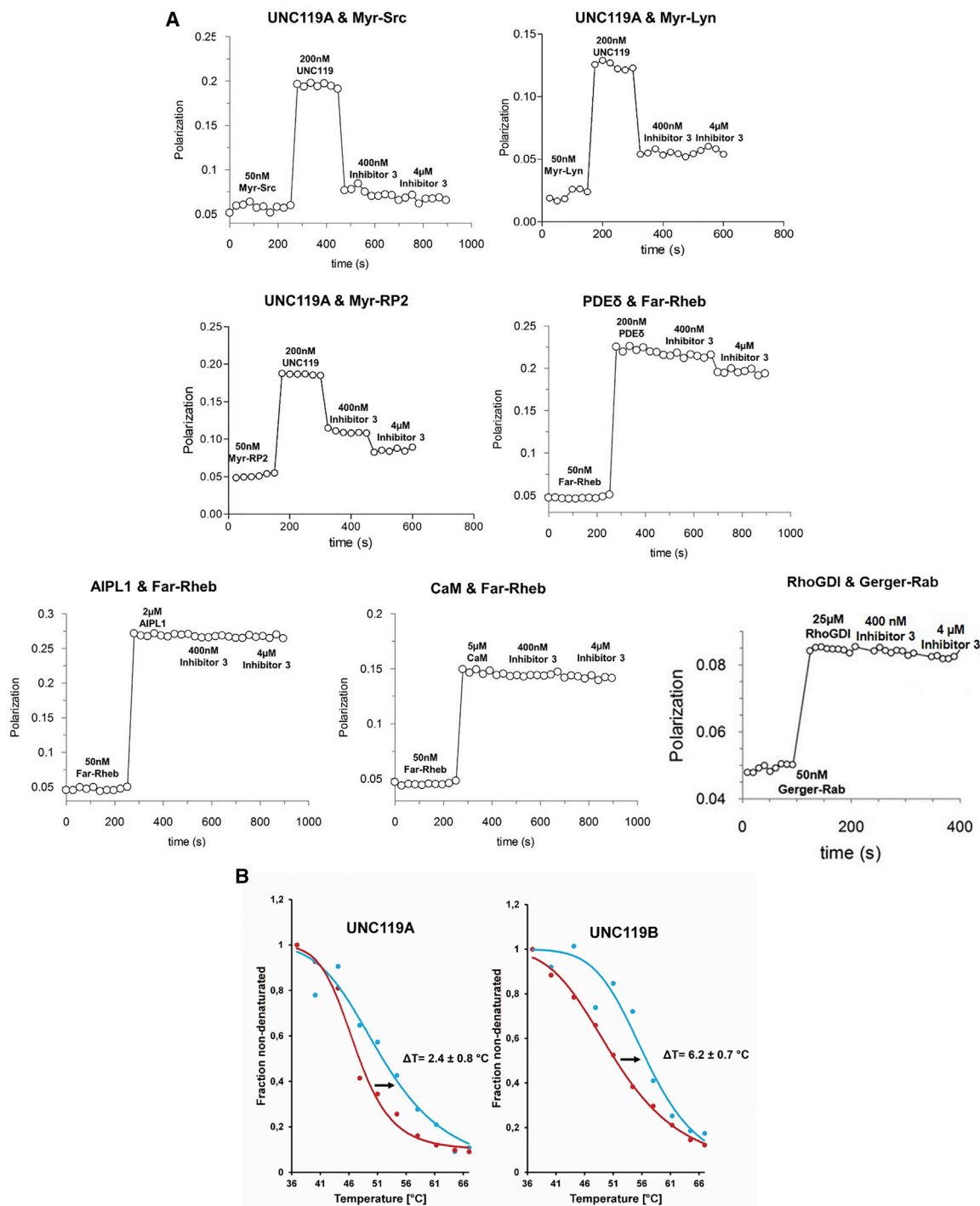


Figure 2. Selectivity and Target Engagement of Compound 3

(A) Fluorescence polarization assay to determine selectivity of compound 3. Fluorescently labeled lipidated peptides (Myr-Src, Myr-Lyn, Myr-RP2, Far-Rheb, or GerGer-Rab) were incubated with the respective binding partner (UNC119A, PDE6 δ , AIPL1, CaM, or RhoGDI). On addition of lipid binder, polarization increased due to the increase of mass. After addition of inhibitor, polarization decreases indicating release of bound peptide.

(B) Cellular thermal shift assay of UNC119 proteins on treatment with DMSO control (red) and compound 3 (blue). Lysates from Jurkat cells were treated with compound 3 at 1 μM , and thermal stabilization of the proteins was identified and quantified by means of tandem mass spectrometry analysis.

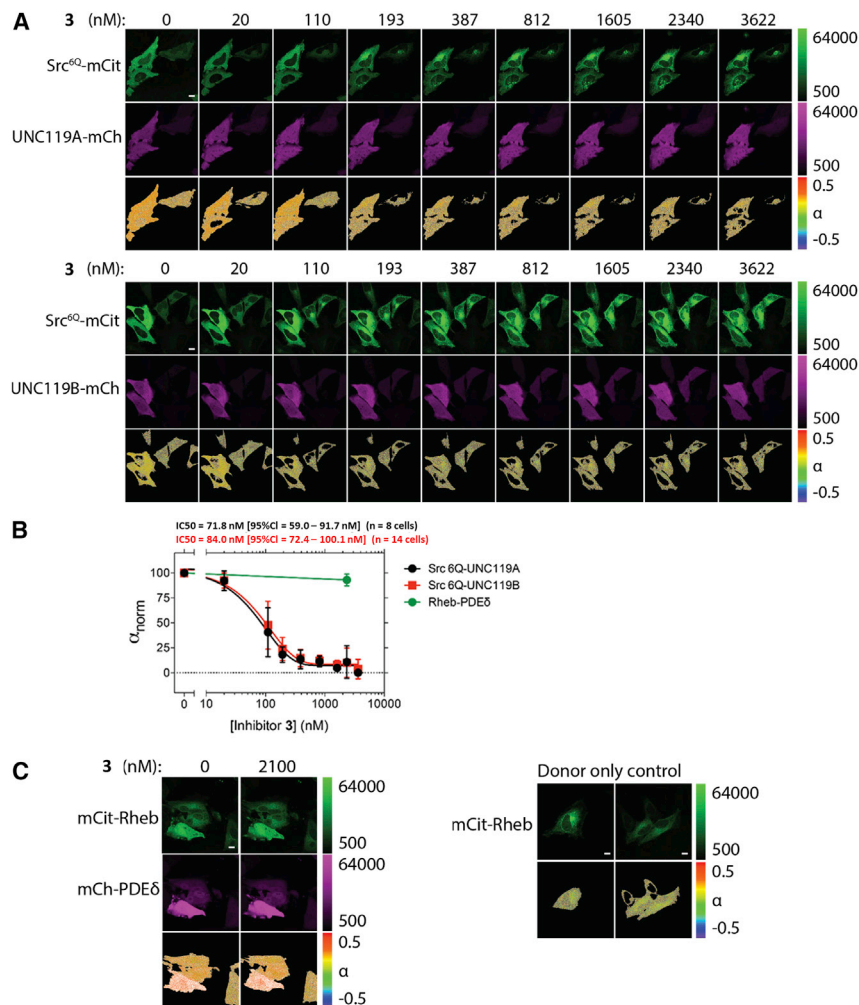


Figure 3. Inhibition of the Interaction between Src and UNC119 Proteins in Cells by Compound 3 Resulting in Redistribution from Cytosol to Endomembranes

(A) FRET-FLIM of the interaction between Src6Q-mCit and UNC119A-mCh (top) or UNC119B-mCh (bottom) in HeLa cells with increasing concentrations of **3**. For each sample, the fluorescence intensity of Src6Q-mCit (donor), the fluorescence intensity of UNC119-mCh (acceptor), and the molar fraction of interacting molecules (α) are shown as per the false-color look-up tables. Inhibitor concentrations are indicated above each image in nM. Scale bars, 10 μ m.

(B) Dose-response graphs. Dose-response curves for cells that reached the final concentration of inhibitor **3** were normalized and then averaged. Curves were fit to an exponential and IC₅₀ calculated on the curve to yield an in-cell K_D of 71.8 nM (95% CI = 59.0–91.7 nM) for UNC119A (n = 8 cells from at least 3 independent experiments) and 84 nM (95% CI = 72.4–100.1 nM) for UNC119B (n = 14 cells from at least 3 independent experiments) for treatment with **3**. The green data points demonstrate that treatment with **3** has no effect on the interaction between Rheb-PDE5 even at the highest concentration of inhibitor (see images in Figure 4C; n = 18 from at least 2 independent experiments). Data are means \pm SD.

(C) Representative FLIM measurements of the mCit-Rheb and mCh-PDE5 interaction with 2.1 μ M of **3**. Upper and middle rows: fluorescence intensity of mCit-Rheb and mCh-PDE5, respectively. Lower rows: molar fraction (α) of interacting mCit-Rheb and mCh-PDE5. Inhibitor concentrations are indicated above each image in nM (n = 18 cells from at least 2 independent experiments). Scale bars, 10 μ m.

endomembranes. Dose-dependent measurements yielded an in-cell K_D (Zimmermann et al., 2013) for UNC119A of 71.8 nM (95% confidence interval [CI] = 59.0–91.7 nM) and an in-cell K_D for UNC119B of 84 nM (95% CI = 72.4–100.1 nM) for compound **3** (Figure 3B). These values were about 6-fold higher than the *in-vitro*-determined IC₅₀ values, which likely reflects restricted availability, e.g., because of aspecific membrane binding of the compound in cells.

These results demonstrate that compound **3** interacts with both isoforms of UNC119 in HeLa cells and inhibits the binding of Src to UNC119. To examine if compound **3** also interferes with the localization of wild-type Src, HeLa cells ectopically expressing Src-mCitrine were treated with distinct concentrations of **3** for 2 h. This resulted in a significant loss of PM localization of Src starting at a concentration of \sim 5 μ M (Figure 4). This relocation occurs at a much higher concentration as the “in-cell K_D” of the compound due to the low entropic equilibration kinetics of Src to all membranes that needs to be matched by a low catalytic turnover of the UNC119/Arl system (Schmick et al., 2015). Importantly, the UNC119-specific inhibitor **3** had no effect on the Rheb-PDE5 interaction, again demonstrating the specificity of the compound (Figures 3B and 3C).

With clear evidence that compound **3** enters cells and interacts with cytoplasmic UNC119 proteins, thereby leading to a depletion of Src from the PM, the response of cells to treatment with the compound was investigated.

Src Y416 Phosphorylation

Inactive Src is phosphorylated at the regulatory tyrosine Y527, while autocatalytic phosphorylation of tyrosine Y416 activates its kinase activity (Patwardhan and Resh, 2010). The second-order reaction of autocatalytic Y416 phosphorylation is dependent on local Src concentration and therefore potentiated by the enrichment of Src on the membrane. Therefore, we investigated the impact of compound **3** on the phosphorylation level of Y416 of Src by means of an in-cell Western assay.

We treated the MDA-MB-231 cells with increasing concentrations of compound **3** for 30 min. We observed that at 78 nM, the phosphorylation of Src (Y416) was reduced by 45.6% \pm 8.7% (Figure 5A). This finding was confirmed by western blot employing HT-29 cells, in which 50 μ M of compound **3** reduced the phosphorylation of Src (Y416) by 56.1% \pm 11% (Figure S4). These data are in accordance with the observations reported for disrupting the interaction between UNC119/Src with Squarunin, which also reduced

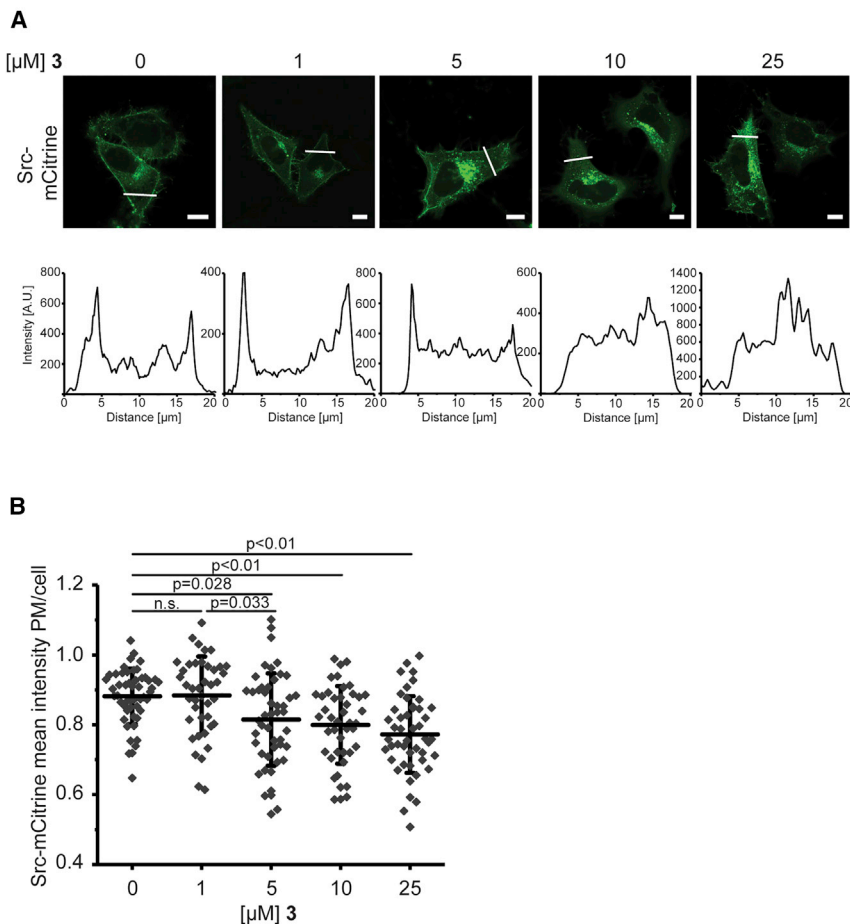


Figure 4. Inhibition of the Interaction between Src and UNC119 Proteins in Cells by Compound 3 Resulting in Loss of Src PM Localization

(A) Representative confocal micrographs of Src-mCitrine distribution in dependence of inhibitor dose (upper row) and corresponding Src-mCitrine intensity profiles along the lines depicted in the micrographs (lower row). Inhibitor concentrations are indicated above each image in μM. Scale bars, 10 μm.

(B) Dot plot of Src-mCitrine mean intensity at the PM over the whole cell dependent on inhibitor dose (n > 41 cells for each condition from 2 independent experiments). Black lines depict mean, error bars depict SD. The p values were calculated using one-way ANOVA.

the phosphorylation of Src (Y416) by ~40% (Mejuch et al., 2017). Partial phosphorylation of Src is likely upheld by residual Src at the PM upon equilibration as well as phosphorylation by other tyrosine kinases.

Clonogenic Assay

To investigate whether disruption of the UNC119-Src interaction with inhibitor **3** and the resulting reduction in Src Y416 phosphorylation leads to an altered growth response, compound **3** was tested in a clonogenic assay (Figure 5B). This assay monitors the survival and proliferation of the cells after compound treatment as reflected in the colony size and colony number, respectively (Klein et al., 2018). Since direct Src inhibition is known to lead to cell growth reduction in triple-negative MDA-MB-231 breast cancer cells because of Src dependency, this cell line was chosen for the clonogenic assay (Sánchez-Bailón et al., 2012). Treatment of the MDA-MB-231 cells with different concentrations of the inhibitor **3** for 10 days led to a significant and dose-dependent reduction in predominantly colony number, which is indicative of the impact of our compound **3** toward cell survival (Figure 5B). To exclude unselective toxicity, the clonogenic assay was performed in SYF cells (Figure 5C), lacking the SFKs Src, Yes, and Fyn, as well as in KRAS-dependent Panc-Tu-1 cells (Figure 5D). In both cases, no colony reduction could be

seen. This showed that our small molecule clearly affected cell survival and cell proliferation of MDA-MB-231 cancer cells but not of cells in which Src was knocked out.

To prove that the observed differences in cell survivability are indeed specific effects of Src inhibition, we engineered an SYF cell line stably expressing constitutive active Src (v-Src) (see the Supplemental Information Figure S5). In these cells, compound **3** administration reduced the viability with increasing inhibitor concentration in clonogenic assays, whereas the colony size, which is a measure of proliferation, was not affected (Figure 6A). To further corroborate

that the expression of constitutive active Src transformed the SYF cells, we performed migration assays in serum-free medium (Figure 6B). Here, the motility of cells expressing constitutive active Src was significantly increased compared with that of parental SYF cells, demonstrating that the expression of constitutive active Src renders these cells motile. Strikingly, this Src-mediated increased motility could be inhibited by administration of 10 μM **3** at the beginning of the measurement (Figures 6B and 6C).

DISCUSSION

In colorectal carcinoma, Src activity increases with disease progression. Enrichment of the N-myristoylated Src-kinase at the cytoplasmic face of the PM drives its activation and interaction with specific effectors (Bjorge et al., 2000; Barker et al., 1995), and is therefore a critical parameter for Src activity. The solubilizing UNC119 proteins interact with myristoylated Src by binding of the lipid moiety within a conserved hydrophobic pocket and mediate spatial cycles that maintain Src localization on the PM (Konitsiotis et al., 2017).

We developed a small-molecule class that binds to UNC119 and disrupts the interaction between UNC119 and myristoylated Src. The most potent low-nanomolar inhibitor is selective for binding to UNC119 as compared with other lipoprotein binding chaperones. We have provided direct proof of binding

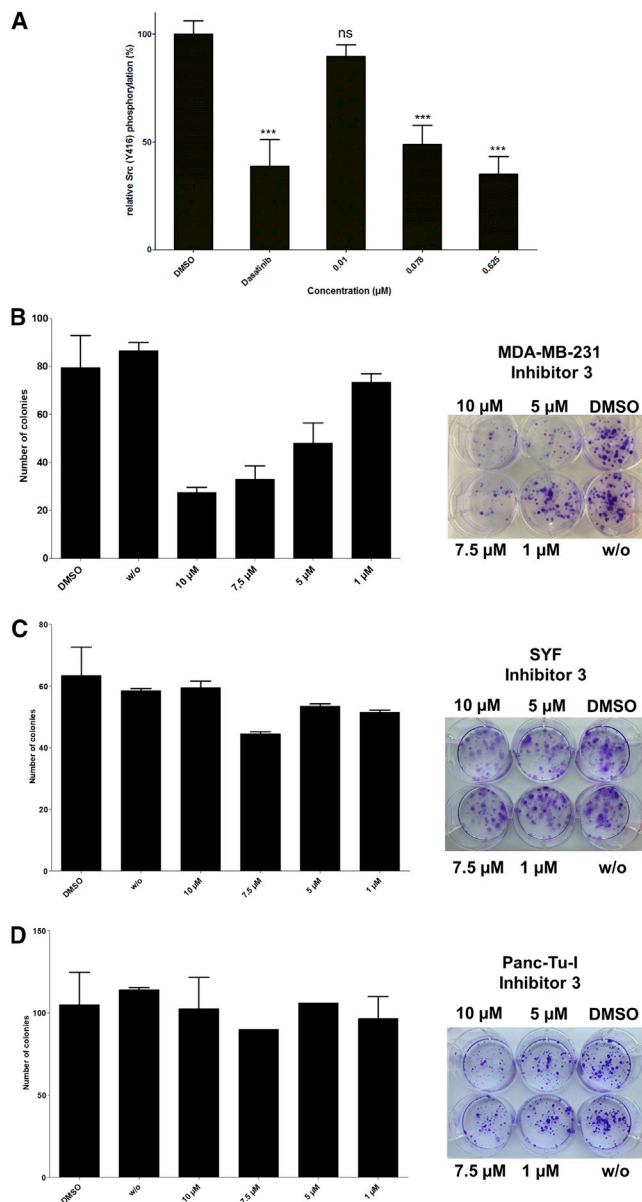


Figure 5. Phosphorylation of Src and Growth Response in Src-Dependent and -Independent Cells upon Disruption of the UNC119/Src Interaction by Compound 3

(A) Concentration dependence of treatment with compound **3** on the phosphorylation level of Src (Y416) as determined by in-cell western assay. The MDA-MB-231 cells were treated with DMSO (1%), **3** (625, 78, and 10 nM), or Dasatinib (78 nM). The amounts of phosphorylated Src were normalized to the total protein. The data are expressed as means \pm SD, the experiment was repeated three times as a quadruplicate. The data were significantly different from untreated DMSO controls (** $p < 0.001$, * $p < 0.01$; ns, non-significant) by Student's *t* test.

(B) Clonogenic assay. MDA-MB-231 cells were treated with indicated amount of inhibitor **3**. Left: quantification of three independent experiments performed as duplicate (means \pm SD). Right: representative clonogenic assay.

(C) SYF cells were treated with indicated amount of inhibitor **3**. Left: quantification of three independent experiments performed as duplicate (means \pm SD). Right: representative clonogenic assay.

in cells to UNC119A and UNC119B using FLIM-FRET. The compound selectively binds to UNC119 in cells. A CETSA experiment further validated the binding in a complex cytoplasmic environment because treatment with compound **3** stabilized both UNC119A and B. Inhibition of the UNC119-Src interaction decreased the level of Src Y416 phosphorylation by $\sim 40\%$ and led to a redistribution of Src from the PM to endomembranes. Notably, small-molecule inhibition of the UNC119-Src interaction manifested itself in a growth inhibitory response and led to reduced number of cell colonies in a clonogenic assay employing triple-negative MDA-MB-231 cells.

Our results demonstrate that small-molecule interference with the dynamics of the spatial Src cycle that maintains it at the PM may open up an opportunity to interfere with oncogenic Src signaling and impair growth of oncogenic Src-bearing cells.

SIGNIFICANCE

UNC119 proteins are involved in cellular trafficking of myristoylated proteins, such as Src, which is considered a highly relevant target in anti-cancer drug discovery. Inhibition of the UNC119-Src interaction is a valid approach to impair UNC119-mediated enrichment of Src at the plasma membrane and to perturb Src signaling. We identified a UNC119-Src inhibitor that interacts with UNC119 proteins in cells. The inhibitor causes Src redistribution to endomembranes, impairs activating Src autophosphorylation on Y419 and reduces growth and clonogenic potential of Src-dependent CRC cells. These findings suggest that small-molecule interference with the dynamics of the Src spatial cycle may open up an opportunity for medicinal chemistry programs targeting cancers with oncogenic Src.

STAR METHODS

Detailed methods are provided in the online version of this paper and include the following:

- KEY RESOURCES TABLE
- CONTACT FOR REAGENT AND RESOURCE SHARING
- EXPERIMENTAL MODEL AND SUBJECT DETAILS
- METHOD DETAILS
 - Compound Synthesis
 - UNC119/Src Small Molecules Library
 - Cellular Thermal Shift Assay
 - Kinetic Solubility Determination
 - Inhibitor Selectivity Assay
 - Clonogenic Assay
 - In-Cell Western Assay
 - Src Localization
 - Generation of Stable v-Src Expressing SYF Cell Line

(D) Panc-Tu-I cells (B) were treated with indicated amount of inhibitor **3**. Left: quantification of three independent experiments performed as duplicate (means \pm SD). Right: representative clonogenic assay.

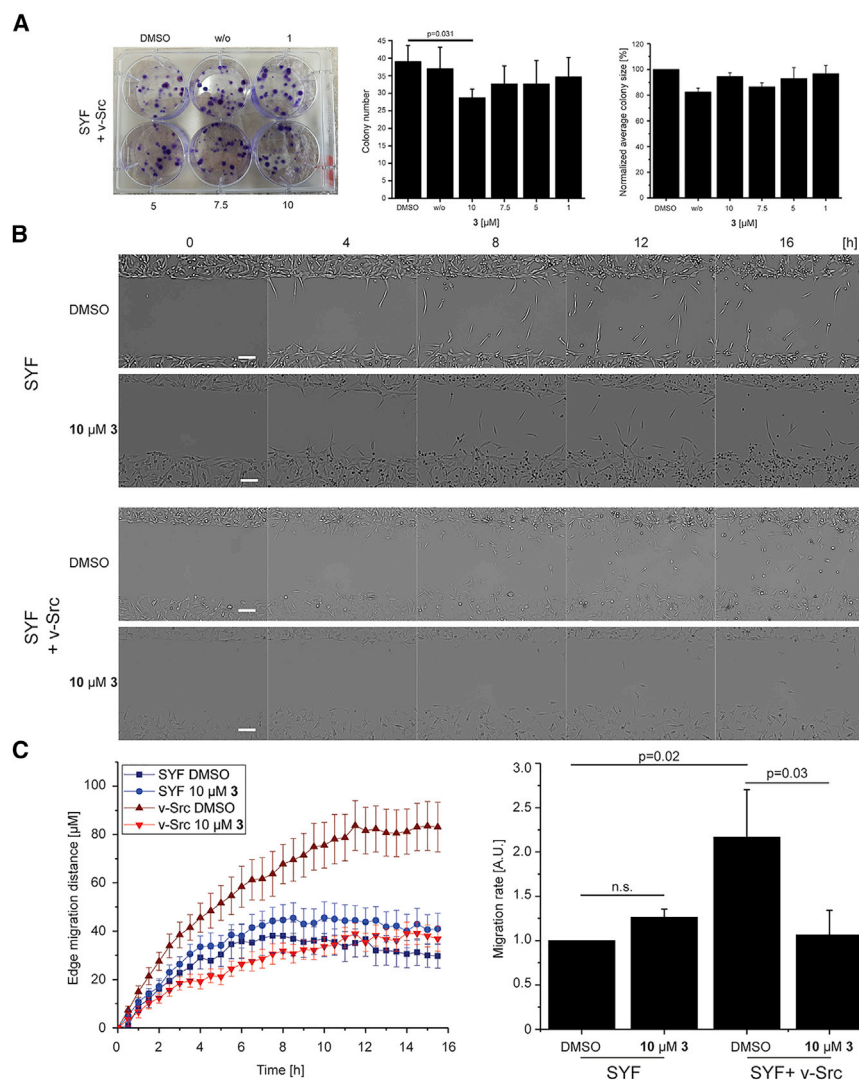


Figure 6. Growth and Migration Inhibitory Responses of Compound 3 Are Src Specific

(A) Representative clonogenic assay of SYF cells stably expressing v-Src treated with indicated amount of inhibitor **3**. Right: quantified colony number and average colony size. The data are expressed as means \pm SD, the experiment was repeated three times.

(B) Representative micrographs of migration assays for SYF cells (upper rows) and SYF cells stably expressing v-Src (lower rows) without or with 10 μ M **3** over time as indicated. Scale bars, 10 μ m.

(C) Left: quantification of the edge migration distance (see the STAR Methods) of SYF and SYF stably expressing v-Src upon administration of 10 μ M **3** or DMSO over time. Right: corresponding migration rates of SYF and SYF stably expressing v-Src. Migration rates were calculated by integration of the area below the edge migration curve and normalized to the SYF DMSO case. The data are expressed as means \pm SEM, the experiment was repeated three times in triplicates. The p values were calculated using one-way ANOVA.

- Cell Migration Assay
- FLIM Experiment
- Western Blot Analysis
- QUANTIFICATION AND STATISTICAL ANALYSIS
- DATA AND SOFTWARE AVAILABILITY

SUPPLEMENTAL INFORMATION

Supplemental Information can be found online at <https://doi.org/10.1016/j.chembiol.2019.02.019>.

ACKNOWLEDGMENTS

Research at the Max Planck Institute of Molecular Physiology was supported by the Max Planck Society and the European Research Council under the European Union's Seventh Framework Program (FP7/2007–2013)/ERC grant agreements nos. 268309 and 322637. The Compound Management and Screening Center (COMAS) Dortmund is acknowledged for performing IC₅₀ determinations in the HTRF-based UNC119 binding assay. We are grateful to Dr. Petra Janning, Dr. Marc Schürmann, Jens Warmers, and Malte Metz (Max Planck Institute of Molecular Physiology) for assistance with the establishment and analysis of CETSA experiments.

T.M. received a Research Scholarship from the Alexander von Humboldt Foundation.

AUTHOR CONTRIBUTIONS

H.W., P.I.H.B., and A.W. conceived the project. H.W. and P.I.H.B. designed the experiments. G.G. performed the chemical synthesis. W.H. and C.K. performed the clonogenic assays. A.K. developed and performed the FRET-FLIM experiments and analysis. C.K. performed the plasma membrane localization studies, generated and characterized the stable v-Src-SYF cells, and performed migration assays. E.F. and N.K. performed the binding selectivity studies and N.K. performed the CETSA experiments. G.G. and T.M. investigated the Src Y416 phosphorylation. T.M. synthesized the peptide probes and developed and established the HTRF-based assay. H.W., P.I.H.B., G.G., W.H., and C.K. wrote the manuscript. All authors commented on the manuscript.

DECLARATION OF INTERESTS

The authors declare no competing interests.

Received: September 14, 2017

Revised: April 19, 2018

Accepted: February 26, 2019

Published: April 4, 2019

REFERENCES

- Allgayer, H., Boyd, D.D., Heiss, M.M., Abdalla, E.K., Curley, S.A., and Gallick, G.E. (2002). Activation of Src kinase in primary colorectal carcinoma: an indicator of poor clinical prognosis. *Cancer* *94*, 344–351.
- Barker, S., Kassel, D.B., Weigl, D., Huang, X., Luther, M., and Knight, W.B. (1995). Characterization of pp60c-src tyrosine kinase activities using a continuous assay: autoactivation of the enzyme is an intermolecular autophosphorylation process. *Biochemistry (Mosc.)* *34*, 14843–14851.
- Bjorge, J.D., Jakymiw, A., and Fujita, D.J. (2000). Selected glimpses into the activation and function of Src kinase. *Oncogene* *19*, 5620–5635.
- Breen, M.E., and Soellner, M.B. (2015). Small molecule substrate phosphorylation site inhibitors of protein kinases: approaches and challenges. *ACS Chem. Biol.* *10*, 175–189.
- Chandra, A., Grecco, H.E., Pisupati, V., Perera, D., Cassidy, L., Skoulidis, F., Ismail, S.A., Hedberg, C., Hanzal-Bayer, M., Venkataraman, A.R., et al. (2011). The GDI-like solubilizing factor PDE δ sustains the spatial organization and signalling of Ras family proteins. *Nat. Cell Biol.* *14*, 148–158.
- Chen, Y.X., Koch, S., Uhlenbrock, K., Weise, K., Das, D., Gremer, L., Brunsveld, L., Wittinghofer, A., Winter, R., Triola, G., and Waldmann, H. (2010). Synthesis of the Rheb and K-Ras4B GTPases. *Angew. Chem. Int. Ed.* *49*, 6090–6095.
- Constantine, R., Zhang, H., Gerstner, C.D., Frederick, J.M., and Baehr, W. (2012). Uncoordinated (UNC)119: coordinating the trafficking of myristoylated proteins. *Vision Res.* *75*, 26–32.
- Franken, H., Mathieson, T., Childs, D., Sweetman, G.M., Werner, T., Tögel, I., Doce, C., Gade, S., Bantscheff, M., Drewes, G., et al. (2015). Thermal proteome profiling for unbiased identification of direct and indirect drug targets using multiplexed quantitative mass spectrometry. *Nat. Protoc.* *10*, 1567–1593.
- Jaiswal, M., Fansa, E.K., Kösling, S.K., Mejuch, T., Waldmann, H., and Wittinghofer, A. (2016). Novel biochemical and structural insights into the interaction of myristoylated cargo with Unc119 protein and their release by Arl2/3. *J. Biol. Chem.* *291*, 20766–20778.
- Keep, N.H., Barnes, M., Barsukov, I., Badii, R., Lian, L.Y., Segal, A.W., Moody, P.C., and Roberts, G.C. (1997). A modulator of rho family G proteins, rhoGDI, binds these G proteins via an immunoglobulin-like domain and a flexible N-terminal arm. *Structure* *5*, 623–633.
- Kim, L.C., Song, L., and Haura, E.B. (2009). Src kinases as therapeutic targets for cancer. *Nat. Rev. Clin. Oncol.* *6*, 587–595.
- Klein, C.H., Truxius, D.C., Vogel, H.A., Harizanova, J., Murarka, S., Martín-Gago, P., and Bastiaens, P.I.H. (2018). PDE δ inhibition impedes the proliferation and survival of human colorectal cancer cell lines harboring oncogenic KRas. *Int. J. Cancer* *144*, 767–776.
- Knight, Z.A., and Shokat, K.M. (2005). Features of selective kinase inhibitors. *Chem. Biol.* *12*, 621–637.
- Konitsiotis, A.D., Roßmannek, L., Stanoev, A., Schmick, M., and Bastiaens, P.I.H. (2017). Spatial cycles mediated by UNC119 solubilisation maintain Src family kinases plasma membrane localisation. *Nat. Commun.* *8*, 114.
- Majumder, A., Gopalakrishna, K.N., Cheguru, P., Gakhar, L., and Artemyev, N.O. (2013). Interaction of aryl hydrocarbon receptor-interacting protein-like 1 with the farnesyl moiety. *J. Biol. Chem.* *288*, 21320–21328.
- Martín-Gago, P., Fansa, E.K., Klein, C.H., Murarka, S., Janning, P., Schürmann, M., Metz, M., Ismail, S., Schultz-Fademrecht, C., Baumann, M., et al. (2017a). A PDE δ -KRas inhibitor chemotype with up to seven H-bonds and picomolar affinity that prevents efficient inhibitor release by Arl2. *Angew. Chem. Int. Ed.* *56*, 2423–2428.
- Martín-Gago, P., Fansa, E.K., Winzker, M., Murarka, S., Janning, P., Schultz-Fademrecht, C., Baumann, M., Wittinghofer, A., and Waldmann, H. (2017b). Covalent protein labeling at glutamic acids. *Cell Chem. Biol.* *24*, 589–597.
- Mejuch, T., van Hattum, H., Triola, G., Jaiswal, M., and Waldmann, H. (2015). Specificity of lipoprotein chaperones for the characteristic lipidated structural motifs of their cognate lipoproteins. *ChemBioChem* *16*, 2460–2465.
- Mejuch, T., Garivet, G., Hofer, W., Kaiser, N., Fansa, E.K., Ehrh, C., Koch, O., Baumann, M., Ziegler, S., Wittinghofer, A., and Waldmann, H. (2017). Small-molecule inhibition of the UNC119-cargo interaction. *Angew. Chem. Int. Ed.* *56*, 6181–6186.
- Papke, B., Murarka, S., Vogel, H.A., Martín-Gago, P., Kovacevic, M., Truxius, D., Fansa, E.K., Ismail, S., Zimmermann, G., Heinelt, K., et al. (2016). Identification of pyrazolopyridazinones as PDE δ inhibitors. *Nat. Commun.* *7*, 11360.
- Parsons, S.J., and Parsons, J.T. (2004). Src family kinases, key regulators of signal transduction. *Oncogene* *23*, 7906–7909.
- Patwardhan, P., and Resh, M.D. (2010). Myristoylation and membrane binding regulate c-Src stability and kinase activity. *Mol. Cell. Biol.* *30*, 4094–4107.
- Reinhard, F.B.M., Eberhard, D., Werner, T., Franken, H., Childs, D., Doce, C., Savitski, M.F., Huber, W., Bantscheff, M., Savitski, M.M., and Drewes, G. (2015). Thermal proteome profiling monitors ligand interactions with cellular membrane proteins. *Nat. Methods* *12*, 1129–1131.
- Roskoski, R. (2004). Src protein-tyrosine kinase structure and regulation. *Biochem. Biophys. Res. Commun.* *324*, 1155–1164.
- Sánchez-Bailón, M.P., Calcabrini, A., Gómez-Domínguez, D., Morte, B., Martín-Forero, E., Gómez-López, G., Molinari, A., Wagner, K.U., and Martín-Pérez, J. (2012). Src kinases catalytic activity regulates proliferation, migration and invasiveness of MDA-MB-231 breast cancer cells. *Cell. Signal.* *24*, 1276–1286.
- Schmick, M., Kraemer, A., and Bastiaens, P.I.H. (2015). Ras moves to stay in place. *Trends Cell Biol.* *25*, 190–197.
- Sperlich, B., Kapoor, S., Waldmann, H., Winter, R., and Weise, K. (2016). Regulation of K-Ras4B membrane binding by calmodulin. *Biophys. J.* *111*, 113–122.
- Talamonti, M.S., Roh, M.S., Curley, S.A., and Gallick, G.E. (1993). Increase in activity and level of pp60c-src in progressive stages of human colorectal cancer. *J. Clin. Invest.* *91*, 53–60.
- Wright, K.J., Baye, L.M., Olivier-Mason, A., Mukhopadhyay, S., Sang, L., Kwong, M., Wang, W., Pretorius, P.R., Sheffield, V.C., Sengupta, P., et al. (2011). An ARL3-UNC119-RP2 GTPase cycle targets myristoylated NPHP3 to the primary cilium. *Genes Dev.* *25*, 2347–2360.
- Zhang, H., Liu, X.H., Zhang, K., Chen, C.K., Frederick, J.M., Prestwich, G.D., and Baehr, W. (2004). Photoreceptor cGMP phosphodiesterase δ subunit (PDE δ) functions as a prenyl-binding protein. *J. Biol. Chem.* *279*, 407–413.
- Zimmermann, G., Papke, B., Ismail, S., Vartak, N., Chandra, A., Hoffmann, M., Hahn, S.A., Triola, G., Wittinghofer, A., Bastiaens, P.I., and Waldmann, H. (2013). Small molecule inhibition of the KRAS-PDE δ interaction impairs oncogenic KRAS signalling. *Nature* *497*, 638–642.

STAR★METHODS

KEY RESOURCES TABLE

REAGENT or RESOURCE	SOURCE	IDENTIFIER
Antibodies		
Rabbit monoclonal anti-Src (36D10)	Cell Signaling Technology	Cat#2109; RRID:AB_2106059
Rabbit monoclonal anti-Phospho-Src (Tyr416) (D4964)	Cell Signaling Technology	Cat#6943; RRID:AB_10013641
Mouse IgG anti-Src	Merck	Cat#05-184 RRID: AB_2302631
donkey anti-rabbit IgG IRDye™ 800	LICOR	Cat# 926-32213 RRID: AB_621848
goat anti-mouse IgG IRDye™ 680	LICOR	Cat#926-68070 RRID: AB_10956588
Mouse anti-GFP	Clontech Laboratories	Cat#632381; RRID:AB_2313808
Mouse monoclonal anti- α -Tubulin	Sigma-Aldrich	Cat#T6074; RRID: AB_477582
Chemicals, Peptides, and Recombinant Proteins		
Acquired compounds	ChemDiv	Cat# see Table S2
TMT label reagents	ThermoFisher Scientific	Cat#90110
DMEM medium	PAN Biotech	Cat#P04-03550
RPMI medium	PAN Biotech	Cat#P04-18047
Fetal bovine serum	Gibco	Cat#10500-084
Sodium pyruvate	PAN Biotech	Cat#P04-43100
Non-essential amino acids	PAN Biotech	Cat#P08-32100
Penicillin-Streptomycin	PAN Biotech	Cat#P06-07100
Odyssey Blocking buffer	LI-COR Bioscience	Cat#927-40000
Src (Myr-GSNKSKPK-Fluorescein)	Mejuch et al., 2015	https://doi.org/10.1002/cbic.201500355
Lyn (Myr-GSIKSK-Fluorescein)	Mejuch et al., 2015	https://doi.org/10.1002/cbic.201500355
RP2 (Myr-GCFFCKRRK-Fluorescein)	Jaiswal et al., 2016	https://doi.org/10.1074/jbc.M116.741827
Rab1 (Fluorescein-SGGGSC(GerGer)-OMe)	Mejuch et al., 2015	https://doi.org/10.1002/cbic.201500355
Rheb (Fluorescein-SQGKSSC(Far)-OMe)	JPT	N/A
UNC119A	Wittinghofer's lab	N/A
PDE6 δ	Wittinghofer's lab	N/A
AIPL1	Wittinghofer's lab	N/A
Calmodulin	Wittinghofer's lab	N/A
Experimental Models: Cell Lines		
Human HeLa (female)	DSMZ	Cat#ACC-57; RRID: CVCL_0030
Murine SYF	ATCC	Cat #CRL-2459; RRID: CVCL_6461
Murine SYF_v-Src	This paper	N/A
Human HT29 (female)	ATCC	Cat#HTB-38; RRID: CVCL_0320
Human MDA-MB-231 (female)	DSMZ	Cat#ACC 732; RRID: CVCL_0062
Human Jurkat (male)	DSMZ	Cat#ACC-282; RRID:CVCL_0065
Human Panc-Tu-I (PaTu-8902) (female)	DSMZ	Cat#ACC-179; RRID:CVCL_1845

(Continued on next page)

Continued

REAGENT or RESOURCE	SOURCE	IDENTIFIER
Oligonucleotides		
Mutagenesis-Primer: v-Src Forward: GTGCTGGAAGTGGCGGAAAAGCTTCG AATTCTGCATGG	This paper	N/A
Mutagenesis-Primer: v-Src Reverse: GCACGCCGGCAGCAGCTGGCCTGC AGTACTCGAA	This paper	N/A
Primer: pPB_v-Src-mCitrine Forward: CGCGTATGGGTAGCAACAAGAGCAAG	This paper	N/A
Primer: pPB_v-Src-mCitrine Reverse: CTCGGCATGGACGAGCTGTACAAGTAAA	This paper	N/A
Recombinant DNA		
Plasmid: Src-mCitrine	Konitsiotis et al., 2017	https://doi.org/10.1038/s41467-017-00116-3
Plasmid: Src6Q-mCitrine	Konitsiotis et al., 2017	https://doi.org/10.1038/s41467-017-00116-3
Plasmids: Unc119A/B-mCherry	Konitsiotis et al., 2017	https://doi.org/10.1038/s41467-017-00116-3
Plasmid: pPB_v-Src-mCitrine	This paper	N/A
Software and Algorithms		
GraFit 5.0	Erithacus Software	http://www.erithacus.com/grafit/
MaxQuant	Cox et al., Max-Planck Institute, Martinsried	https://www.biochem.mpg.de/5111795/maxquant
MRI Wound Healing Tool	ImageJ	http://dev.mri.cnrs.fr/projects/imagej-macros/files
GraphPadPrism 6.0	GraphPad	https://www.graphpad.com/scientific-software/prism/
Image Studio	LI-COR	https://www.licor.com/bio/products/software/image_studio/
Other		
Odyssey Fc imaging system	LI-COR	https://www.licor.com/bio/products/imaging_systems/odyssey_fc/
Spark multimode microplate reader	Tecan	https://lifesciences.tecan.com/multimode-plate-reader

CONTACT FOR REAGENT AND RESOURCE SHARING

Further information and requests for resources and reagents should be directed to and will be fulfilled by the lead contact, Herbert Waldmann (herbert.waldmann@mpi-dortmund.mpg.de).

EXPERIMENTAL MODEL AND SUBJECT DETAILS

The female human cell line MDA-MB-231, the female human Panc-Tu-I cell line, murine cell line SYF and the murine stable v-Src expressing SYF cell line were cultured in Dulbecco's Modified Eagle's medium (DMEM) supplemented with 10% fetal bovine serum, 1 mM sodium pyruvate and 1% (v/v) non-essential amino acids. The male human Jurkat cell line was cultivated in RPMI 1640 medium supplemented with 10% fetal bovine serum 1 mM sodium pyruvate, 1% (v/v) non-essential amino acids and 1% PenStrep. The female human HT-29 cell line was maintained in Ham's medium supplemented with 10% fetal bovine serum and 1 mM L-glutamine. All cell lines were maintained at 37°C and 5% CO₂ in humidified atmosphere.

METHOD DETAILS

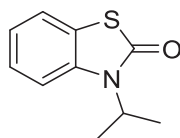
Compound Synthesis

Reagents were obtained from either Sigma-Aldrich (Taufkirchen, Germany) or AlfaAesar (Karlsruhe, Germany) and used without further purification. Solvents were purchased from Fisher Scientific. Dry solvents were purchased from Acros. Drying of compounds was performed in high vacuum (3×10^{-1} mbar). TLC plates, Polygram Sil G/UV 254 from MACHEREY-NAGEL GmbH & Co. KG (Dürren, Germany), were used for detection of reaction process. Analytical HPLC-MS chromatograms were obtained from an Agilent HPLC (1100 series) using a reversed phase column (C4 or C18 – 5 μ m, 250x4.6 mm) equipped with a Finnigan LCQ ESI spectrometer and an UV/VIS detector (flow rate: 1.0 ml/min; time: 15 min; using 0.1 % HCOOH in H₂O, and 0.1 % HCOOH in MeCN). Purification was performed by dry packed silica columns or preparative HPLC. Silica gel 60 (0.04-0.063 mm) was purchased from MACHEREY-NAGEL GmbH & Co. KG (Dürren, Germany). Preparative HPLC purification was performed in an Agilent HPLC (1100 series) using a reversed-phase C18 column. Measurements of nuclear magnetic resonance were performed on a Bruker Avance 400 at r.t.

The calibration standards are the indicated deuterated solvents. Following abbreviations for coupling are made: s=singlet, d=doublet, t=triplet, q=quintet, m=multiplet. High resolution mass spectra (HRMS) were measured on a Thermo Orbitrap coupled to a Thermo Accela HPLC system (HPLC column: Hypersyl GOLD, 50 mm x 1mm particle size 1.9 μ m) using electrospray ionization (ESI). HPLC traces were determined using Shimadzu Shim-pack XR-ODS 2.2 μ m, 2.0 i.d.*50mm column (method: H₂O/ACN (0.1% formic acid) from 90/10 to 0/100 over 2.5 minutes, then 0/100 for 1.25 min, 90/10 for 1.25 min).

UNC119/Src Small Molecules Library

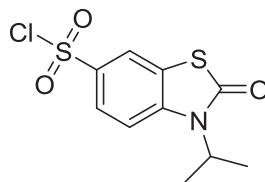
3-isopropylbenzo[d]thiazol-2(3H)-one



2(3H)-Benzothiazolone (1.0 g, 6.6 mmol, 1.0 eq) was dissolved in dry DMF (16 mL) under an argon atmosphere. 2-iodopropane (0.70 mL, 7.0 mmol, 1.1 eq) was added dropwise. The reaction mixture was cooled to 0°C prior addition of NaH (0.37 g, 7.92 mmol, 1.2 eq). The reaction was stirred for 3 h at reflux. The resulting mixture was washed with brine and extracted three times with DCM. The organic phase was dried over Na₂SO₄, concentrated under high vacuum and purified by column chromatography using EtOAc/cyclohexane (1:1) (0.79 g, 60 %).

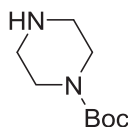
¹H NMR (400 MHz, CDCl₃): δ = 7.30 (d, J = 7.8 Hz, 1H), 7.21 (t, J = 7.8 Hz, 1H), 7.13 (d, J = 8.2 Hz, 1H), 7.04 (t, J = 7.6 Hz, 1H), 4.73 (dt, J = 13.8, 6.9 Hz, 1H), 1.50 (d, J = 7.0, 6H).

3-isopropyl-2-oxo-2,3-dihydrobenzo[d]thiazole-6-sulfonyl chloride



To chlorosulfonic acid (12.0 eq.), 3-isopropylbenzo[d]thiazol-2(3H)-one (0.9 mmol, 1.0 eq) was added slowly at 0°C under an argon atmosphere. The mixture was stirred at 0°C for 20 min, and at 70°C for 7 h. The mixture was carefully quenched onto ice (10 mL) under vigorous stirring. The precipitated crude was extracted with EtOAc (3 x 20 mL). The combined organic layers were dried over MgSO₄, filtered and concentrated under reduced pressure. The crude product was used without purification in the next step. Due to its poor stability in water, no ESI-MS data could be obtained.

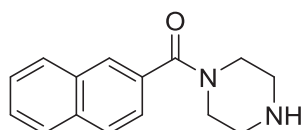
tert-butyl piperazine-1-carboxylate



To a solution of piperazine (2.4 g, 27.9 mmol, 1.0 eq) in dry DCM, was added dropwise a solution of di-tert-butyl dicarbonate, (3.0 g, 13.4 mmol, 0.5 eq) in dry DCM. The reaction mixture was stirred for 1 day until completion of the mono protected piperazine. The solution was washed with water and brine to extract the unreacted starting material. The solvent was removed under reduced pressure to afford the desired compound as a white solid (3.7 g, 72%).

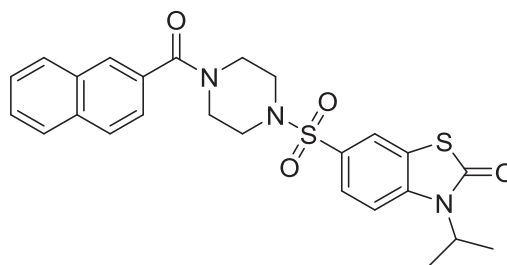
¹H NMR (CDCl₃, 400 MHz) δ 3.54 (t, 4H, J = 4.9 Hz), 3.03 (t, 4H, J = 4.7 Hz), 1.26 (s, 9H).

naphthalen-2-yl(piperazin-1-yl)methanone



Tert-butyl piperazine-1-carboxylate (3.7 g, 19.9 mmol, 1.0 eq) and 2-naphthoylchloride (5.7 g, 29.9 mmol, 1.5 eq) were mixed in dry DCM (15 mL). Then, Et₃N (4.2 mL, 29.9 mmol, 1.5 eq) was added dropwise at 0°C. The reaction mixture was allowed to warm up to r.t and stirred o/n. The reaction mixture was washed with water and brine. The organic phase was dried under Na₂SO₄ and concentrated under reduced pressure. The crude compound was solved in a mixture of DCM/TFA 1:1 (50 mL). The reaction was stirred at r.t for 2 h until full deprotection of the starting material (monitored by TLC and ultra-HPLC). Toluene was added to the mixture and the solvents were co-evaporated under reduced pressure. The desired compound was obtained as an oil (2.88 g, 59 % over 2 steps) and used for the next step without further purification.

6-((4-(2-naphthoyl)piperazin-1-yl)sulfonyl)-3-isopropylbenzo[d]thiazol-2(3H)-one



Naphthalen-2-yl(piperazin-1-yl)methanone (0.5 g, 2.10 mmol, 1.0 eq) and 3-isopropyl-2-oxo-2,3-dihydrobenzo[d]thiazole-6-sulfonyl chloride (0.61 g, 2.10 mmol, 1.0 eq) were solved in pyridine (5 mL) and stirred at 70°C for 5 hours. The solvent were removed under high vacuum and the crude was purified by preparative HPLC (H₂O/ACN + 0.1% TFA) to afford the desired compound **GG-211** (150 mg, 75%).

HR-ESI-MS: $m/z = 496.1371$ ($[M + H]^+$, calcd. for C₂₅H₂₆O₄N₃S₂⁺: 496.1359).

¹H NMR (400 MHz, DMSO): $\delta = 8.14$ (d, $J = 1.8$ Hz, 1H), 7.96 – 7.92 (m, 3H), 7.75–7.65 (m, 1H), 7.60 – 7.52 (m, 1H), 7.45 (dd, $J = 8.6, 1.4$ Hz, 1H), 7.27 – 7.21 (m, 1H), 7.18 – 7.10 (m, 2H), 4.88 – 4.79 (m, 1H), 3.54 (s, 4H), 3.02 (s, 4H), 1.50 (d, $J = 6.9$ Hz, 6H).

¹³C NMR (400 MHz, DMSO): $\delta = 175.25, 169.22, 141.11, 133.83, 133.32, 132.83, 131.87, 129.57, 128.88, 128.69, 128.33, 127.86, 127.38, 125.99, 125.17, 123.79, 123.43, 121.78, 113.54, 62.83, 40.87, 40.66, 40.45, 40.24, 20.24, 19.65$.

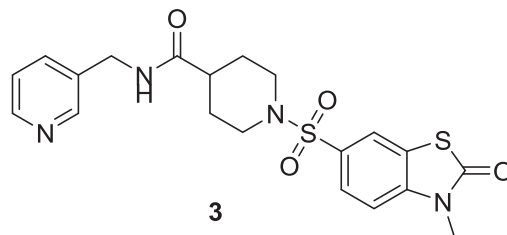
Preparative HPLC: C18 column using 5 % (ACN + 0.1 % TFA) to (100 % ACN + 0.1% TFA) over 52 minutes. $t_R = 24$ min.

LC-MS trace: 2.27 min

Commercially Available Compounds

Compounds used for the UNC119/Src chemical library were purchased from ChemDiv® (For Cat# see Table S2). The molecular weight and the UV traces of all the compounds were controlled by ESI-MS and the selected top compound was checked by ¹H NMR and HR-MS in house.

Compound **3** (ChemDiv®, Catalog Number: #L306_1198).



Compound **3** (5.3 mg) was obtained as a white powder from ChemDiv®. Analytical data were verified in-house before screening and further biological evaluation.

HR-ESI-MS: $m/z = 475.1465$ ($[M + H]^+$, calcd. for C₂₂H₂₆N₄O₄S₂⁺: 475.1468). ($\Delta = 0.59$ ppm)

¹H NMR (400 MHz, CDCl₃): data in accordance with the supplier.

HPLC traces: 1.31 min

Cellular Thermal Shift Assay

Cell Lysis

Jurkat cells were harvested by centrifugation at 350 g for 5 min and washed twice with PBS. Cells were re-suspended in PBS prior to lysis by freeze-thaw cycles. Insoluble cell components were precipitated by centrifugation at 100000 g for 20 min at 4°C in an ultra-centrifuge (Optima MAX-XP). The lysate was snap-frozen and stored at –80°C until further use.

Thermal Denaturation

Thawed lysate was diluted with PBS buffer to a protein concentration of 2 mg/ml to a total volume of 2.9 ml. The diluted lysate was split into two aliquots of 1.4 ml each. One sample was treated with the compound, resulting in a final concentration of 1 μ M compound and 1% DMSO. The vehicle sample was treated with an equal amount of DMSO (final concentration of 1%). The compound and vehicle sample were incubated at ambient temperature for 10 min prior to splitting into 10 aliquots of 120 μ l. Aliquots were heated at a temperature gradient of 37 - 67°C in a the PCR cycler (Eppendorf Mastercycler ep gradient S) for 3 min. One vehicle sample was always heated in parallel with one compound sample. Subsequently, samples were cooled to 4°C and centrifuged at 100000 g for 20 min at 4°C in an ultracentrifuge (Optima MAX-XP). The supernatant (100 μ l) was transferred into low binding Eppendorf tubes.

Trypsin Digest

75 μ l of each aliquot were treated with freshly prepared buffer A (100 mM triethylammonium bicarbonate buffer (TEAB); 75 μ l) and buffer B (200 mM tris(2-carboxyethyl)phosphine (TCEP), 0.2 mM TEAB; 7.5 μ l) and incubated for 1 h at 55°C. A freshly prepared solution of 375 mM iodoacetamide in water was added to each sample followed by incubation for 30 min in the dark. Subsequently, 900 μ l of pre-cooled acetone were added to precipitate the proteins overnight at -20°C. Samples were centrifuged at 8000 g for 10 min at 4°C, pellets were air dried for 1.5 h and re suspended in 100 mM TEAB. Trypsin (0.4 μ g/ μ l in 10 mM HCl) was added to the samples and digestion was performed at 37°C overnight.

TMT Labeling

The TMT label reagents (TMT10plex, #90110 ThermoFisher Scientific) were equilibrated at room temperature and each label was dissolved in 82 μ l anhydrous acetonitrile. Each DMSO- or compound-treated sample was then incubated with one of the TMT label reagents so that given TMT label codes for one temperature of the used temperature gradient. After incubation for 2 h at ambient temperature an aqueous hydroxylamine solution was added to each vial and incubation continued for another 15 min. All aliquots of the compound- or the DMSO-treated samples respectively were combined and evaporated to dryness in a centrifugal evaporator at 30°C.

pH Fractionation and nanoHPLC Analysis

Samples were dissolved in 120 μ l ammonium formate (NH₄COO, 20 mM, pH 11), ultrasonified for 2 min at the ambient temperature and vortexed for 1 min, followed by centrifugation at 13000 rpm for 3 min at 20°C. Subsequently, 110 μ l of the supernatant were transferred into a polypropylene sample vial (250 μ l, SUN-Sri 200046, 12x32 equipped with a 6820.0028 lid from Thermo Scientific). The peptides were fractionated using an XBridge C18 column (130 3.5 μ m 1.0 x 150 mm) on a Thermo Scientific Ultimate 3000 (LPG-3400MB, TCC-3000SD, WPS- 3000TBFC ANALYTICAL, VWD-3100). Solvent A (20 mM NH₄COO in water, pH 11) and solvent B (20 mM NH₄COO in water with 60 % acetonitrile). The gradient was adjusted in order to achieve ideal separation into 10 new fraction samples. Between the different runs the column was washed with blank runs to avoid carry over from vehicle to compound samples. After fractionation the samples were evaporated to dryness in a centrifugal evaporator at 30°C. For nanoHPLC-MS/MS analysis the samples were dissolved in 20 μ l of 0.1% TFA and 3 μ l were injected into the nanoHPLC-MS (Thermo Scientific Ultimate 3000 (SRD-3400, NCS-3500RS NANO, WPS-3000TPL-RS, VWD-3400RS, Thermo Scientific QExactive Plus mass spectrometer). The samples were injected onto a pre-column cartridge (5 μ m, 100 Å, 300 μ m ID * 5 mm, Dionex, Germany). The eluent was 0.1 % TFA in water with a flow rate of 30 μ l/min. The precolumn was flushed with the eluent for 5 min, followed by transfer of the sample from the pre-column to the PepMap100 RSLC C18 nano-HPLC column (2 μ m, 100 Å, 75 μ m ID x 25 cm, nanoViper, Dionex, Germany) using a linear gradient starting with 95 % solvent A (water containing 0.1 % formic acid) / 5 % solvent B (acetonitrile containing 0.1 % formic acid). Over a time of 125 min with a flow rate of 300 nl/min, the gradient was increased to 60 % solvent A 0.1 % formic acid / 40 % solvent B. The nano-HPLC was online coupled to the Quadrupole-Orbitrap Mass Spectrometer using a standard coated SilicaTip (ID 20 μ m, Tip-ID 10 μ m, New Objective, Woburn, MA, USA). Mass range of m/z 300 to 1650 was acquired with a resolution of 70000 for full scan, followed by up to ten high energy collision dissociation (HCD) MS / MS scans of the most intense at least doubly charged ions using a resolution of 35000 and a NCE energy of 35 %.

Data Evaluation

Data evaluation was carried out with MaxQuant software3 (v.1.5.3.30) including the Andromeda search algorithm, based on the Uniprot database as a reference for the human proteome. The search criteria were a full enzymatic trypsin cleavage with tolerance for two miscleavages. Carbamidomethylation was set as a fixed modification. Oxidation of methionine and acetylation of the N-terminus were set as variable protein modifications. For relative quantification the type "reporter ion MS2" was chosen and for all lysine residues and peptide N-termini 10plex TMT labels were defined. The mass accuracy for full mass spectra was set to 20 ppm (first search) and 4.5 ppm (second search), respectively and for MS/MS spectra to 20 ppm. For peptide and protein identification a false discovery rate of 1 % was chosen. Only proteins for which at least two peptides were quantified were chosen for further validation. Relative quantification of proteins was performed using the reporter ion MS2 algorithm implemented in MaxQuant.

Melting Curves Calculation

The difference in melting point between compound and vehicle was determined based on an inhouse developed Excel-Macro. Therefore, the amount of non-denaturated protein was determined by the reporter ion intensity and normalized to the lowest temperature, which was adjusted to 1. The relative fold changes were calculated as a function of temperature. The measuring points were fitted according to the following equation using an iterative working macro for Microsoft Excel.

$$y = \text{bottom plateau} + \frac{(\text{top plateau} - \text{bottom plateau})}{1 + e^{-\left(\frac{a}{\text{Temp}}\right)^{-b}}}$$

Top plateau value is fixed to 1; Temp is the temperature of the sample; bottom plateau is a protein specific constant that defines the maximal denaturation; **a** and **b** are constants which describe the curve progression. The melting point of a protein is defined as the temperature at which half of the protein has been denatured. This point aligns with the inflection point of the curve. For hit identification following requirements were defined and had to be fulfilled for all replicates: (1) the protein has to be identified with at least two unique peptides, (2) the DMSO control has to melt nicely, i.e. the TMT labels of the two highest temperatures have to have a relative intensity of smaller or equal of 35 % of the label of the highest temperature, (3) the shifts of the melting points for the same protein have to exhibit a consistent stabilization or destabilization of at least 3°C.

Kinetic Solubility Determination

10 mM DMSO stocks of the inhibitors were diluted to a final concentration of 500 μ M in aqueous Hepes buffer (50 mM pH 7.4) and incubated for 90 min while vigorously shaking at room temperature. Following filtration of the solution, the relative kinetic solubility of test compounds in aqueous buffer was calculated by measuring the spectrophotometric absorbance between 250 and 500 nm and comparing the recorded absorbance value to the absorbance of the compound in the 50% acetonitrile solution as the high control (= 500 μ M).

Inhibitor Selectivity Assay

For determining the ability of inhibitor **3** to displace lipidated cargo from different chaperones the following chaperone-lipidated peptide pairs were used: UNC119A-Src, PDE6 δ -Rheb, AIPL1-Rheb and calmodulin-Rheb. The peptides Src (Myr-GSNKSKPK-Fluorescein), Lyn (Myr-GSIKSK-Fluorescein), RP2 (Myr-GCFFCKRRK-Fluorescein) and Rab1 (Fluorescein-SGGGSC(GerGer)-OMe) were prepared according to the previously reported method. Rheb peptide (Fluorescein-SQGKSSC(Far)-OMe) was purchased from JPT. All the measurements were carried out at 20°C in a buffer containing 30 mM Tris, pH 7.5, 150 mM NaCl, 3 mM DTE (for the measurements with calmodulin, 10 mM CaCl₂ was added to the buffer). The fluorescently labelled lipidated peptides were placed in the cuvette. The corresponding chaperone proteins UNC119A (200 nM), PDE6 δ (200 nM), AIPL1 (2 μ M), calmodulin (5 μ M) or RhoGDI (25 μ M) were added. Increasing concentrations of inhibitor **3** (400 nM and 4 μ M) were added to the protein-peptide complex and the changes in the fluorescence polarization were recorded at the excitation and emission wavelengths of 495 nm and 520 nm corresponding to the fluorescein-labeled peptides. Data analysis was done with GraFit 5.0 program (Erithracus Software).

Clonogenic Assay

MDA-MB-231 (500 cells/well), Panc-Tu-1 (500 cells/well) or SYF (250 cells/well) were seeded in a six well plate in DMEM medium. Adhesion took place over night (16 h). 10 mM DMSO containing stock solution was added and according DMSO amount was added to adjust the same DMSO concentration in all wells. Medium with inhibitor was exchanged all two to three days. After 10 days, media was washed with PBS. 500 μ l 4% paraformaldehyde in PBS was added and incubated for 20 minutes. Afterwards, paraformaldehyde was aspirated and 1000 μ l 0.1 % crystal violet in PBS (stock: 5 % crystal violet in EtOH) was added and incubated for 20 minutes at room temperature. Subsequently, the wells were washed with 1x PBS (1, 5 and 10 minutes). All experiments were performed as duplicates of biological triplicates. The plates were dried overnight. Photos were taken and analysed with ImageJ.

In-Cell Western Assay

The ICW assay was performed using the Odyssey Imaging System (LI-COR,) according to the manufacturer's instructions. MDA-MB-231 cells grown in a 384-well plate (2×10^4 cells/well) were incubated with different inhibitors and concentrations for 30 minutes. Afterwards, cells were fixed using paraformaldehyde, washed, permeabilized with 0.1% Triton X-100 and blocked overnight at 4°C in LICOR buffer. The cells were stained for 2h at room temperature with mouse IgG antibody against Src (1:400, Merck) together with rabbit IgG antibody against phospho-Src (Tyr416) (1:400, Cell Signaling Technologies) in LICOR buffer. Subsequently, the cells were washed and stained with donkey anti-rabbit IgG IRDye™ 800 antibody (1:1000; LI-COR Biosciences) and goat anti-mouse IgG IRDye™ 680 antibody (1:1000; LI-COR Biosciences). Protein expression was quantified using the Odyssey Imaging System. For statistical analyses, integrated intensities of fluorescence in wells were determined using software provided with the imager station (LI-COR). The relative amount of phosphorylated Src was obtained by normalizing to the amount of total Src in all experiments. All experiments were performed as quadruplicate and three biological replicates.

Src Localization

HeLa cells (1000 cells/well) were plated on eight-well LabTec plates (Thermo Fisher Scientific) and transiently transfected with Src-mCitrine (Konitsiotis et al., 2017). One day after transfection, cells were treated with distinct concentration (1 – 25 μ M) of inhibitor **3** for 2 h. Subsequently, cells were washed with PBS and fixed with 4 % PFA in PBS. Confocal images were acquired with a confocal laser-scanning microscope (FV1000, Olympus). For detection of Src-mCitrine, the sample was excited using the 488 nm wavelength of an argon laser. Fluorescence was collected through an oil immersion objective ($\times 60/1.35$ UPlanSApo, Olympus) and spectrally filtered by a band pass filter from 500 - 550 nm. To assess the spatial Src distribution, cells were segmented into three concentric areas with an outer area containing the plasma membrane and two inner areas containing mostly cytoplasm. Each segment had a width of one third of all pixels of circularized cells (Konitsiotis et al., 2017). The mean intensity of the plasma membrane segment was normalized to the total mean intensity of each cell.

Generation of Stable v-Src Expressing SYF Cell Line

Human v-Src was generated by C-terminal substitution of the human c-Src sequence in a Src-mCitrine expression plasmid (Konitsiotis et al., 2017) from FLEDYFTSTEPQYQPGENL to QLLPACVLEVAE using a Q5[®] Site-Directed Mutagenesis Kit (NEB) according to the manufacturer's protocol. After sequence validation, the mutated v-Src-mCitrine construct was cloned into a PiggyBac vector (System Bioscience) utilizing the restriction enzymes MluI and SpeI (NEB). Afterwards, SYF cells were co-transfected with the above described construct and a PiggyBac transposase (System Bioscience, ratio 1:1) to enable genome integration. Stable transfected cells were selected based on puromycin resistance, which is also encoded by the PiggyBac expression plasmid.

Cell Migration Assay

SYF and SYF stably expressing v-Src were seeded into 2-well silicone culture-inlets, which create a cell-free area in between, in fibronectin-coated 12-well culture dishes. Cells were starved two hours before the start of the measurement and the inlet was removed immediately before the start. Images were acquired using an Olympus IX81 inverted microscope through a 10x/0.16 NA air objective. Transmission images were acquired every 30 min for 16 h. During each experiment, three fields of view were imaged for each condition. Segmentation of the cell-free area was performed using the MRI Wound Healing plugin in ImageJ. The average distance D between the two cell layer edges was calculated as follows:

$$D = A/(L*2)$$

where A is the cell-free area between the edges and L is the length of the cell-free area. The length of the cell-free area is assumed to be constant, since no cells migrated into the field of view from these sites. The distance has to be additional divided by factor 2, because the cells migrate in from both edges. The edge migration distance in μm was calculated by subtracting the obtained distance for any time point ($D_{t=}$) from the initial distance at the beginning ($D_{t=0}$). The migration rate was determined by integration of the edge migration distance curves.

FLIM Experiment

FLIM experiments were carried out at 37°C and 5% CO₂ on a Leica SP5 confocal microscope equipped with a Picoquant FLIM module (LSM Upgrade Kit/SMD Module, Picoquant). mCitrine fluorescence was excited at 514 nm with a pulsed supercontinuum laser with a repetition rate of 40 MHz. Photons from the mCitrine channel were detected using avalanche photodiodes and arrival times were processed by a time-correlated single-photon counting module (PicoHarp 300, Picoquant). Intensity thresholds were applied to segment the cells from the background fluorescence. Global analysis of FLIM-FRET data was implemented using Matlab R2014A (The Mathworks Inc., MA, USA) to obtain images of the molar fraction (a) of interacting SFK-mCit with UNC119-mCh. Pixels with a total number of photons less than a pre-set threshold of 50 counts were excluded from the analysis.

Western Blot Analysis

Cells were washed once with ice-cold PBS and lysed on ice with RIPA-buffer (20mM Tris pH 7.5, 150mM NaCl, 0.5mM Na₂ EDTA, 1 % sodium deoxycholate, 0.1% sodium dodecyl sulfate, 1% IGEPAL supplemented with Complete Mini EDTA-free protease inhibitor (Roche Applied Science) and 1% phosphatase inhibitor cocktail 2 and 3 (P5726 and P0044, Sigma Aldrich). After 10 min, cells were scraped off and centrifuged at 14000g for 20 min at 4°C. SDS-polyacrylamide gel electrophoresis was carried out with 10 μg of whole-cell lysate. The gels were blotted onto polyvinylidene difluoride membrane (PVDF, Millipore) and blocked for 1 h at room temperature. The following antibodies were used for western blotting in the stated dilution: anti-Src (Cell Signaling Technology, 1:1000), Phospho-Src (Y416) (Cell Signaling Technology, 1:1000), GFP (Clontech Laboratories, 1:1000), α -Tubulin (Sigma Aldrich, 1:3000) and matching secondary infrared antibodies IRDye 800 donkey anti rabbit IgG, IRDye 680 goat anti mouse IgG, (LI-COR, 1:10000). Blots were scanned on a LI-COR Odyssey imaging system.

QUANTIFICATION AND STATISTICAL ANALYSIS

Data from independent experiments are presented as mean values \pm standard deviation (SD) or mean values \pm standard error of the mean (SEM), which is depicted in the figure legends together with the number of technical and biological replicates. Data fitting was performed using GraphPad Prism 6.0. Details to descriptive quantifications can be found in figures, their respective legends and tables. The data significantly different from untreated DMSO controls (***) indicates $p < 0.001$, ** indicates $p < 0.01$, ns: non-significant) were quantified by Student's t-test or by one-way ANOVA (Data analysis were performed using Prism[®] software).

DATA AND SOFTWARE AVAILABILITY

The employed software is listed in the respective experimental sections and the [Key Resources Table](#).